Journal of Climate Change
ISSN 2395-7611 Volume 12 (2026) No. 2. pp.412–431

https://doi.org/10.70917/jcc-2026-024

Article

Investigation of Global MPPT Technique for Sustainable Solar PV Systems Under Partial Shading

Y.T.R.Palleswari [1,*], Asapu Siva [1], Pothula Jagadeesh [2], Susitra D [3], K. P. Swaroop [1] and Lakshman Kumar Dangeti [1]

[1] Dept. of Electrical & Electronics Engineering, Shri Vishnu Engineering College for Women, Bhimavaram, Andhra Pradesh,534202, India
[2] Dept. of Electrical & Electronics Engineering, S.R.K.R Engineering College, Bhimavaram, Andhra Pradesh, 534204,India
[3] Dept. of Electrical & Electronics Engineering, Sathyabama Institute of Science and Technology, Chennai, Tamil Nadu, 600119,India
* Correspondence author: tulsiadabala@svecw.edu.in

Abstract: The shading effect arises when a photovoltaic system experiences an uneven incident solar irradiance due to obstructions. In such situations, cells receiving lower solar irradiance levels may absorb power instead of generating it. To mitigate this impact and safeguard solar panels, bypass diodes are employed. Partial shading, where only a part is shaded from the Photo Voltaic (PV) module, can have more severe consequences than uniform shading. Shading poses challenges to Maximum Power Point Tracking (MPPT) algorithms. MPPT is designed to make sure the photovoltaic system is operating at its peak power, but shading can make the system converge to a local extreme when compared to the global maximum. To overcome this challenge, a Globalized MPPT algorithm is taken, which comprises three components which are Partial Shaded Detection, searching for Global peak, and an MPPT procedure. Moreover, DC-DC converters are crucial in solar systems to efficiently convert variable DC voltage from solar panels to a stable voltage. Considering this context, a high-gain converter is essential for elevating voltage levels, eliminating the need for a transformer on the AC side. While prior research has explored various derived DC-DC converters to achieve larger gains, this often necessitates an increase in the number of components. To address this challenge, a hybrid high-gain DC-DC converter is used which have fewer components and lower voltage stress.

The operational features are obtained using PSCAD/EMDTC software and analyzed comprehensively. Eventually, to authorize the working of globalized MPPT approach with the High gain converter during different scenarios, the simulation was executed systematically and the performance characteristics are presented.

Keywords: Globalized MPPT 1; DC-DC Converter 2; Partial shading 3; High Gain Converter 4.

1. Introduction

To meet the growing energy demand, the world is looking towards renewable energy resources mainly on solar and wind due to their clean power generation, reduced greenhouse gas emissions and low maintenance requirements (J. Kumar et al.,2020;Palleswari et al.,2021). Out of all the available energy resources, Solar PV power generation is one of the thriving renewable energy sectors because it is environmentally friendly, produces no noise, pollution free and with improved advancement in power electronics and semiconductor technologies. Moreover, from a few years the cost per kilowatt rating is also diminished. But the main drawback of PV systems is their strong reliance on irradiance and temperature which makes the I–V and P–V characteristics nonlinear (Eltawil et al.,2013) thus reducing the output power. Maximum Power Point Tracking (MPPT) is essentially needed to obtain the maximum power from the PV system by designing and implementing a controller.

Perturb and Observe (P&O), Fractional Short-Circuit Current (FSCC), Constant Voltage (CV) and Incremental Conductance (IC) are the few MPPT methods among numerous approaches (Suresh et al.,2023;Esram et al.,2007). In addition to these few advanced methods based on soft computing are also used. All the MPPT techniques differ in various factors, including effectiveness, complexity, sensor requirements, ease of hardware integration, and the speed of convergence (Mohanty et al.,2014). The utmost used MPPT is Perturb and Observe (P&O), primarily due to its simplicity, user-friendliness and Accuracy (Forouzesh et al.,2018). Its straightforward algorithm makes it popular for many photovoltaic systems, offering an effective solution for tracking the MPP (Maximum Power Point). The algorithm is effective under standard atmospheric conditions but troubles during change in the atmosphere such as partial shading to track the Global peak on the P-V curve, instead it settles at local peak (Ahmed et al.,2018). Enormous papers have been published partial shading condition (Mohanty et al.,2016;Shang et al.,2018;Soedibyo et al.,2017;Titri et al.,2017;Pendem et al.,2018;Rezaii et al.,2018;Goud et al.,2019;Madhu et al.,2019;Alshareef et al.,2022;Bingöl et al.,2018). But few fail to track the Global point, some given poor performance etc., So, to address this issue, a Global MPPT (GMPPT) algorithm is used in this paper to obtain the peak power under varying atmospheric conditions.

In addition, power converters play a crucial role in PV energy systems (Taheri et al.,2012). Not only obtain good efficiency and boosted voltage but also for better control and protection, DC-DC converters are preferred option (Alex et al.,2017). In previous studies, numerous researchers have proposed various types of derived DC-DC converters aimed at obtaining higher voltage gains (Shahir et al.,2018;Smadi et al.,2017; Bharathi et al.,2022;Andrade et al.,2018;Arima et al.,2019;Krishna et al.,2021;Bekkam et al.,2021;Lee et al.,2019;Arfin et al.,2019;Faraji et al.,2019).But the main problem with them is that in few converters, component count is high, some suffers with high voltage stress and some have less efficiency. As a result, a high gain DC-DC converter with reduced component count and voltage stress is used. The Hybrid High Gain Converter (HHGC) is evaluated to achieve optimum efficiency from the solar PV system with the Globalized MPPT algorithm under EMTDC software.

2. Hybrid High Gain DC-DC Converter

Figure 1 illustrates the Circuit diagram of the Hybrid high gain converter. In this structure, a dual-boost topology is synergistically integrated with a quadratic converter to realize enhanced voltage gain with a least component count. It uses two number of inductors, four capacitors and five number of diodes and only one switch.

The power flow of the converter is accomplished by the semiconductor switches and the regulation of the output is done by the proper adjustment of the duty cycle. More over inductor and capacitor are for reducing the ripples and for getting uniform output.

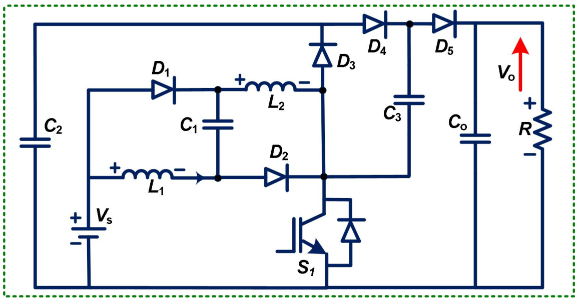

Figure 1. Circuit diagram of Hybrid High gain DC-DC converter.

The 2 modes of operation of the converter are Continuous Current Conduction Mode (CCM) and Discontinuous Current Conduction Mode (DCM). The operational waveforms for CCM and DCM modes are obtained by the conduction and interruption phases of the switching devices.

2.1. CCM Operation

It is having 2 modes again.

Mode 1: During the ON condition of the switch, the inductor L_1 and L_2 gets charged simultaneously and during the same period, through the switch, the energy of C_2 is released to C_3 which shows that the voltage across C_3 is increasing as the energy is fed back to it from previous cycle also. Currently, the output receives energy from C_O. Under these operating conditions, the corresponding circuit is clearly portrayed in Figure 2(a). With the switch in ON condition, the inductor and capacitor voltages are related as:

$$\begin{aligned} V_{L1} &= V_{L2} = V_s \\ V_{C1} &= V_s \\ V_{C3} &= V_{C2} \end{aligned} \tag{1}$$

Mode 2: Over the duration of the state when switch S_1 is off, the deposited energy in the inductor L_1, L_2, and capacitor C_1, C_3 are discharged toward the load and at that instant, the capacitor C_O gets charged to transfer the energy at which switch is in ON state.

Mode 2 operational circuit is as shown in Figure 2(b) where the capacitor C_2 is charged to the voltages of Vs, V_{L1}, V_{C1} and V_{L2}. The corresponding relations are as:

$$V_{L1} + V_{L2} = V_s + V_{C1} + V_{C3} - V_o \tag{2}$$

Gain value can be obtained as:

$$G = \frac{V_o}{V_s} = \frac{4}{(1-D)} \tag{3}$$

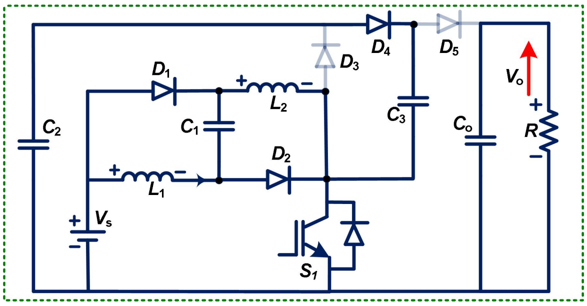

(a) Mode 1

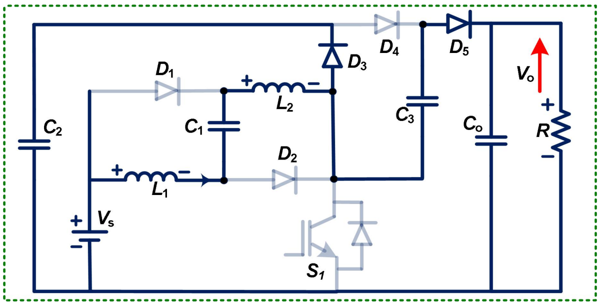

(b) Mode 2

Figure 2. Operating Circuit of the High-Gain DC–DC Converter.

2.2. DCM Operation

As the inductor size is small, Prior to the completion of operation within a cycle, current approached to zero, hence inductor will get charged to the maximum value yielding to high voltages at the load terminals. The voltage output reaches to intense value but there is a decline in the converter's performance. Hence, choosing a perfect value of inductor is highly needed to achieve the operation.

With the selection of mode, the error signal is produced by comparison of reference current with actual measured current and is given as an input to the Proportional Integral (PI) controller to generate the switching pulses which is necessary to swath on the power switch. As the inductor size is small, Prior to the completion of operation within a cycle, current approached to zero, hence inductor will get charged to the maximum value yielding to high voltages at the load terminals. The voltage output reaches to intense value but there is a decline in the converter's performance. Hence, choosing a perfect value of inductor is highly needed to achieve the operation.

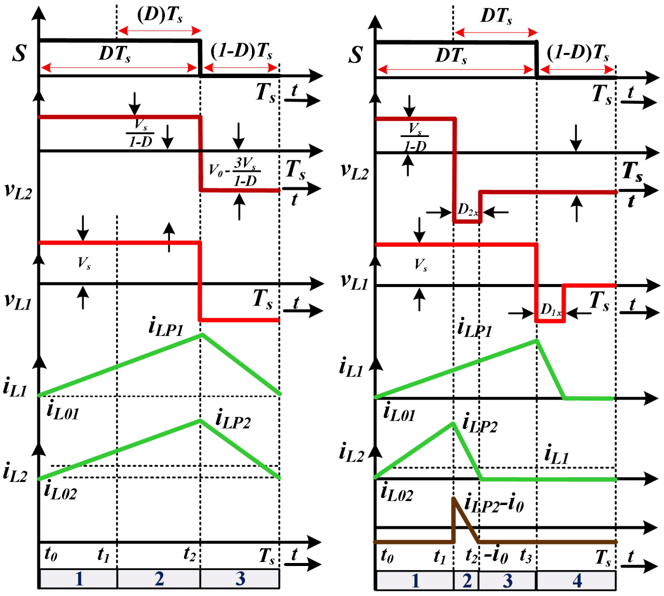

Figure 3. Waveforms of the DC-DC converter under Hybrid high gain operation.

Figure 3 is about the converter waveforms. The voltage and current characteristics of different devices associated with the inductor are presented to describe the energy transfer mechanism. The uniform operation of the converter can be observed through the presented graphs.

The expression for load-current is given as:

$$\frac{(dV_s)^2 T_s}{(2V_s - V_{C2} - V_o)L} = \frac{V_o}{R} \tag{4}$$

In DCM conditions, up on simplification the gain ratio is presented as:

$$G_{dcm} = \frac{D}{1-D} + D\sqrt{\frac{D}{(1-D)^2} + \frac{1}{\tau_L}} \tag{5}$$

Also, the inductor time constant is given as:

$$\tau_L = \frac{D^2(1-D)^2}{4-2D} \tag{6}$$

Using (6), the operating state of the converter can be analyzed by plotting the corresponding graph. Using (5), the standardized inductor constant has been found and it varies with respect to Duty Ratio(D). The frontier section of CCM and DCM process are revealed in Figure 4.

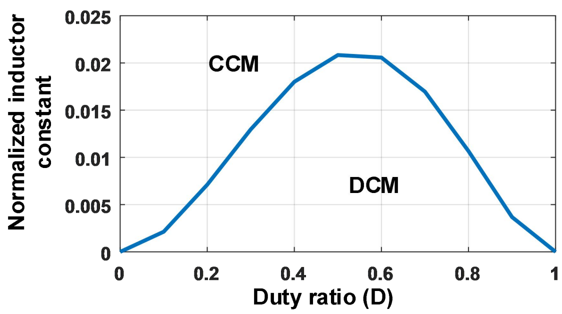

Figure 4. CCM and DCM operating range in relation to duty ratio.

The LCL filter is employed to address harmonic distortion issues that may arise during the energy exchange process. Disturbances occurred by harmonic components leads to degradation of power quality, resulting in irregular power transmission which will influence the stable operation of the network. With the use of LCL filter, by suppressing the unwanted harmonic contents, the power quality can be enhanced and enables a smoother, more reliable exchange of power between the micro-grid and the utility grid.

2.3. Simulation and Results of High Gain Converter

For validation of converter's effectiveness, a computational model was constructed in the PSCAD environment, and the performed simulated analysis are presented here. The PSCAD simulation circuit is shown in Figure 5. All the switching components and the associated control circuits required for the converter are included in the simulation. To observe the energy transfer of the converter in each interval, appropriate switching pulses are applied.

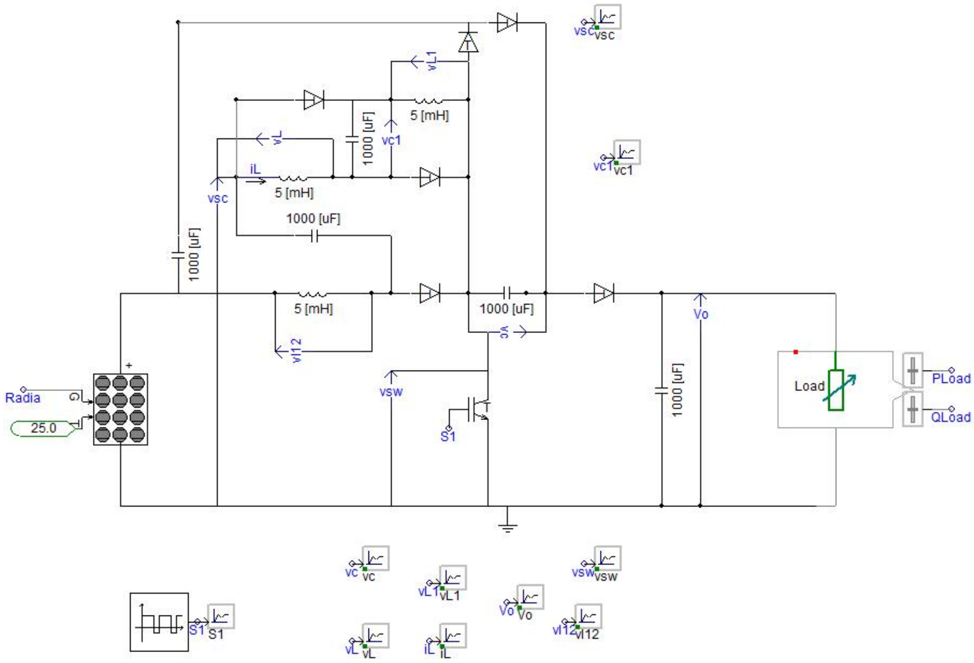

Figure 5. PSCAD simulation circuit diagram of High gain DC-DC converter.

Figure 6(a) and (b) shows that the change in inductor voltage is based on the charging and discharging of the inductor current and is dependent on the duty ratio as well as current waveforms of inductor and capacitor, output voltage are shown as in Figures 7-9.

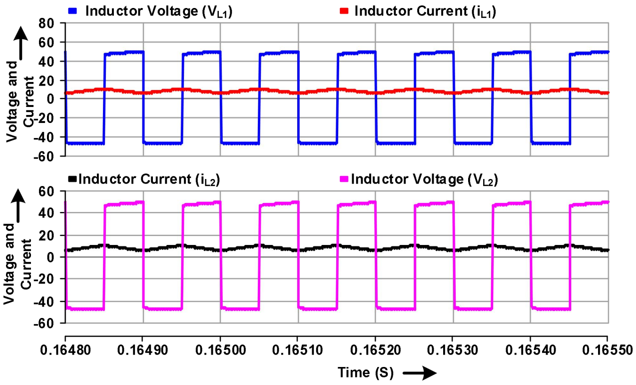

(a) Voltage and current of the Inductor

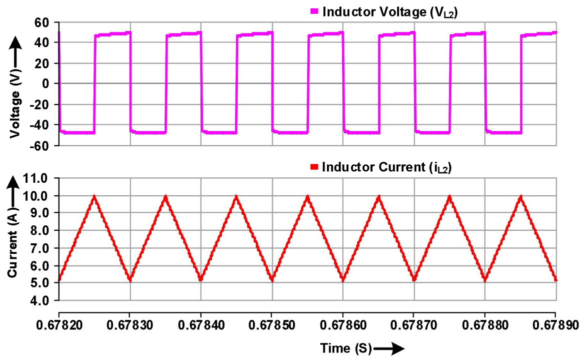

(b) Projected view of voltage and current of the inductor

Figure 6. Simulated outcomes.

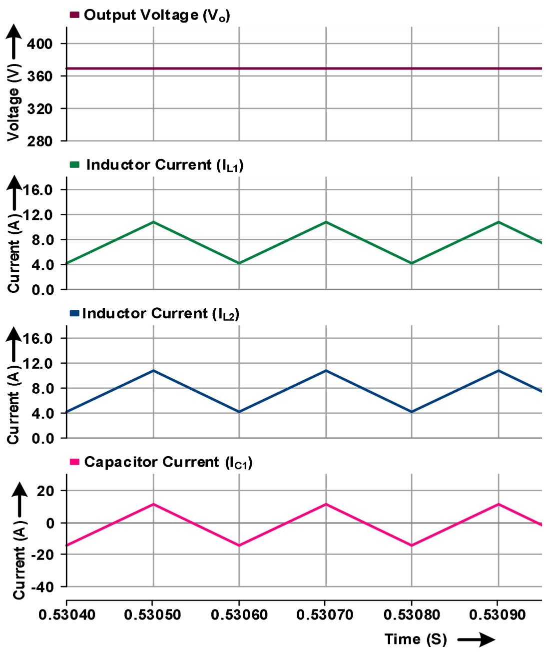

Figure 7. Simulation results of voltage output, currents across inductor and capacitor.

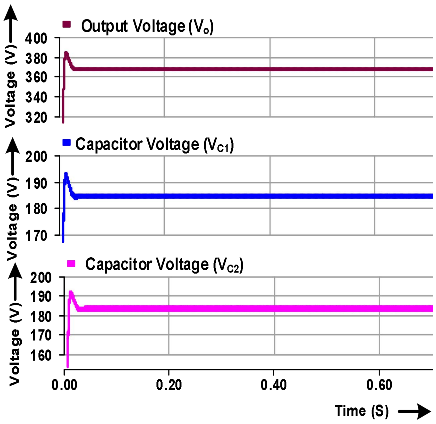

Figure 8. Voltage responses of C1 and C2 and the output obtained from simulation.

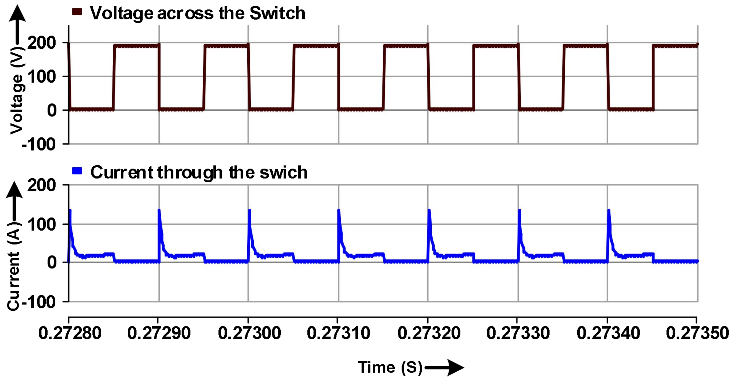

Figure 9. Impact of voltage and current loading on the device.

3. Hardware Implementation of High Gain Converter

To validate the functioning possibility of the converter, the findings through experimentation are also obtained and the experimental setup. Experimental investigations are performed to assess the converter performance under steady-state as well as dynamic operating conditions. The results obtained shows the effectiveness of the converter suitability for practical PV systems. The voltage across inductor and the capacitor were noted experimentally and shown in Figure 10.

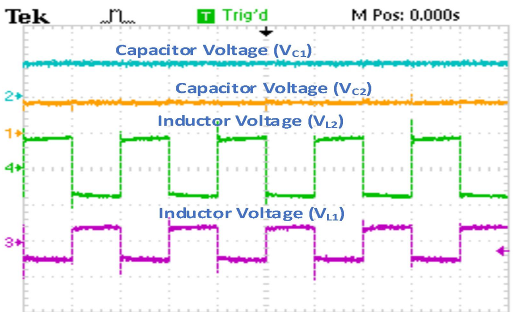

Figure 10. Voltage output and voltage across the inductor and capacitor through experimental setup.

The voltages across V_{L1}, V_{C1}, and V_{C3} are summed up to obtain the output voltage and is shown in the Figure 11.

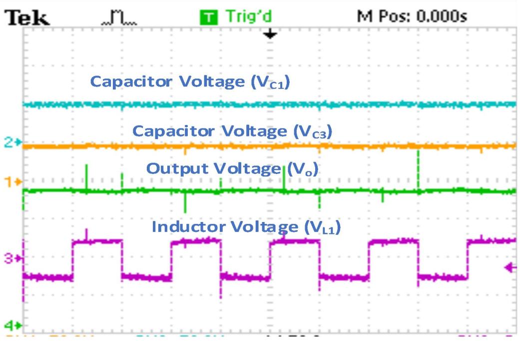

Figure 11. Experimental results of voltage output, and voltage across inductor and capacitor.

The converter functionality and its performance are verified through the responses obtained through experimental validation of the output voltage and inductor current as in Figure 12. The converter's operation is verified as in Figure 13 in DCM.

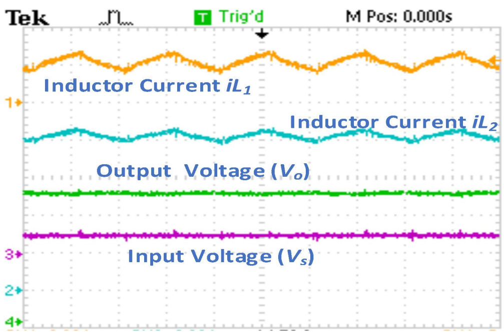

Figure 12. Results of Inductor current and voltage across Inductor through Experimentation.

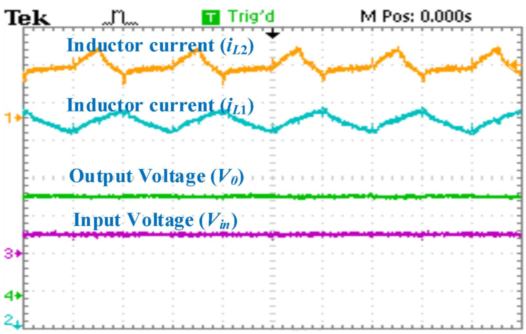

Figure 13. Inductor current and voltage under DCM through Experimentation.

4. Globalized MPPT controller

4.1. The GMPPT operation

A clear representation of the Globalized MPPT approach is provided through the block diagram in Figure 14.

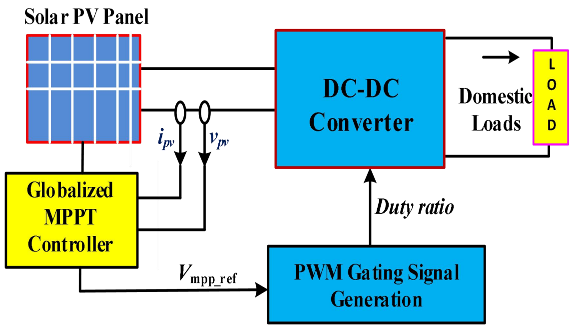

Figure 14. Block diagram of Globalized MPPT approach.

The GMPPT operation begins by incorporating traditional P&O, GMPPT, and multiple step functions. Their integration into the algorithm ensures efficient and effective performance. Flowchart of the approach is as shown in Figure 15. During partial shading, a timer trigger redirects control from the primary algorithm to locate the new global MPP, V_{UMPP} (t).

The scheme begins by determining the series and parallel connected panels in total. It then gathers data from the previous operating cycle, such as the peak power point (P_{MPP}) and the corresponding voltage (V_{MPP}), to locate the voltage and MPP on the I-V and P-V curves. At this stage, the generated voltage and current instantly is V'_{PV} (t) and I'_{PV} (t) (stage 7) With these instants above and by the used method, V'_{UMPP} (t) (stage 8) will be known which are the updated values of global MPP point.

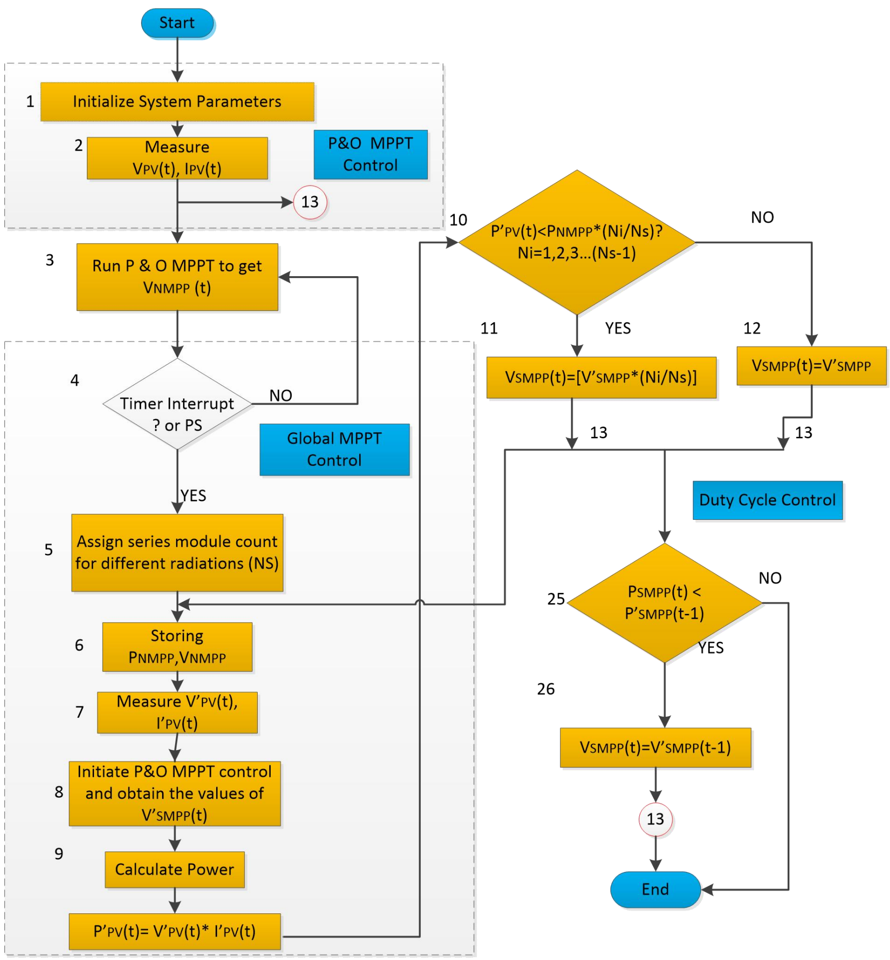

Figure 15. Globalized MPPT algorithm in Flowchart.

Initially, the power at the instant is to be calculated by P'_{PV} (t) = V'_{PV} (t) * I'_{PV} (t) (state 9), fluctuations in power are to be noticed i.e., if P' (t) < $P_{GMPP}\times$ (Ni/NS) (state 10) to verify the efficacy of the MPPT operation. Now by upholding the mentioned conditions, the voltage of the MPP at the instant will be

V_{SMPP} (t) = V'_{SMPP} (t) * (Ni/NS) (state 11), else, V_{SMPP} (t) will be V'_{SMPP} (t) (state 12). Depending up on the irradiation value, generated power will be same and continuous till the above conditions are satisfied. Then command will be moved to duty ration control unit to obtain the actual power generation. Here, GMPP controller supports to obtain the variation of power from the generated. If the value is negative, then initiates the next perturbation, otherwise goes with the earlier duty ratio. (P_{SMPP}(t)<P'_{SMPP}(t-1), then V_{SMPP}(t) = V'_{SMPP}(t-1)).

4.2. Duty ration control

To receive peak power from the PV array, the controller determines an appropriate duty ratio for operation. The operational sequence is illustrated in Figure 16, where the process initiates by acquiring V_{UMPPV} from states 11, 12, or 26 corresponding to partially shaded regions of the solar PV array, while V_{NMPPV} is obtained from state 3 associated with the unshaded condition (state 13).

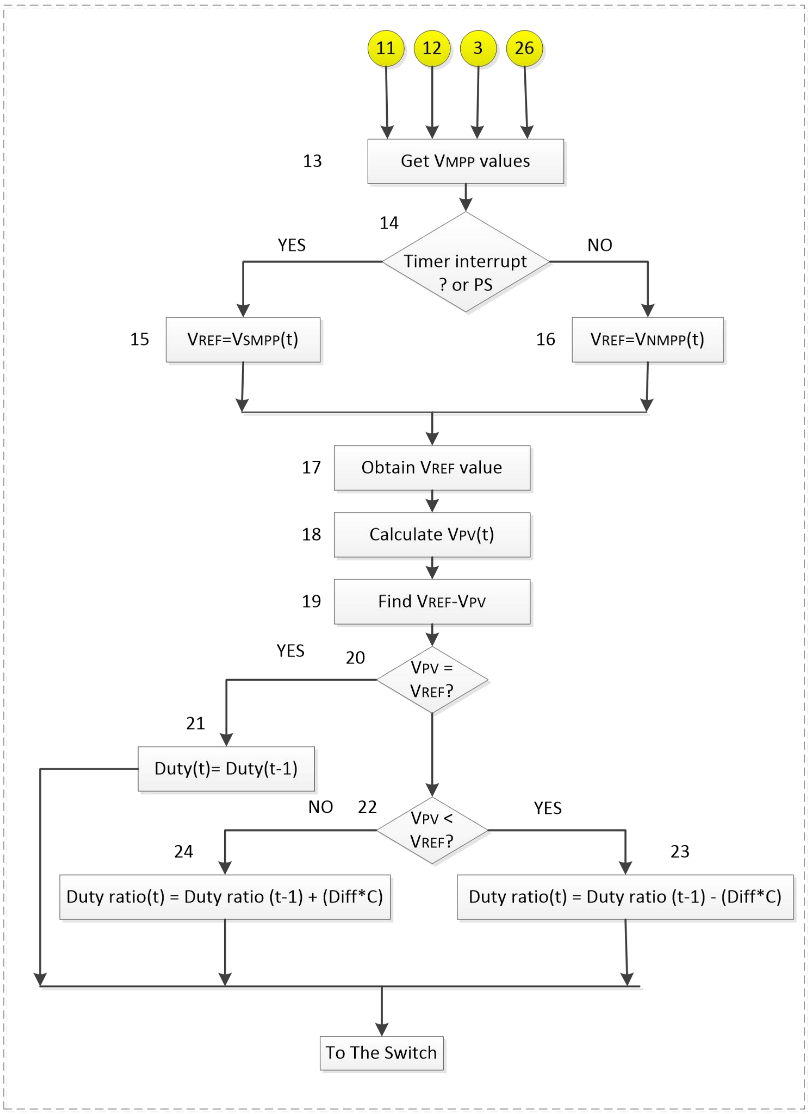

Figure 16. Control Flow Diagram for Duty Ratio Adjustment in Partially Shade PV Arrays.

From state 14, the disrupted condition is found. If the condition is true, then the voltage to be taken as reference will be V_{UMPP} (t) (state 16), otherwise it was V_{NMPP} (t) (state 15). The process will be taken forward till the error gets zero and the value of duty ratio must be corrected, if not continue with the same duty ratio as previous. If the voltage reference is equal to V_{PV} (state 20), D_{new} = D_{t-1} (state 21), The duty cycle D is varied within the range of 0 to 1 (states 23 & 24). Across the operating states (5 to 26), iterative adjustment of the duty ratio is executed, thereby enabling high-precision MPPT performance even under partially shaded conditions. To execute computational study, solar panels are connected in series. By connecting 10 modules in series for each string with several strings in parallel, the solar PV array is formed. The PSCAD simulation diagram is as in Figure 17 and Table 1 shows the required simulation parameters.

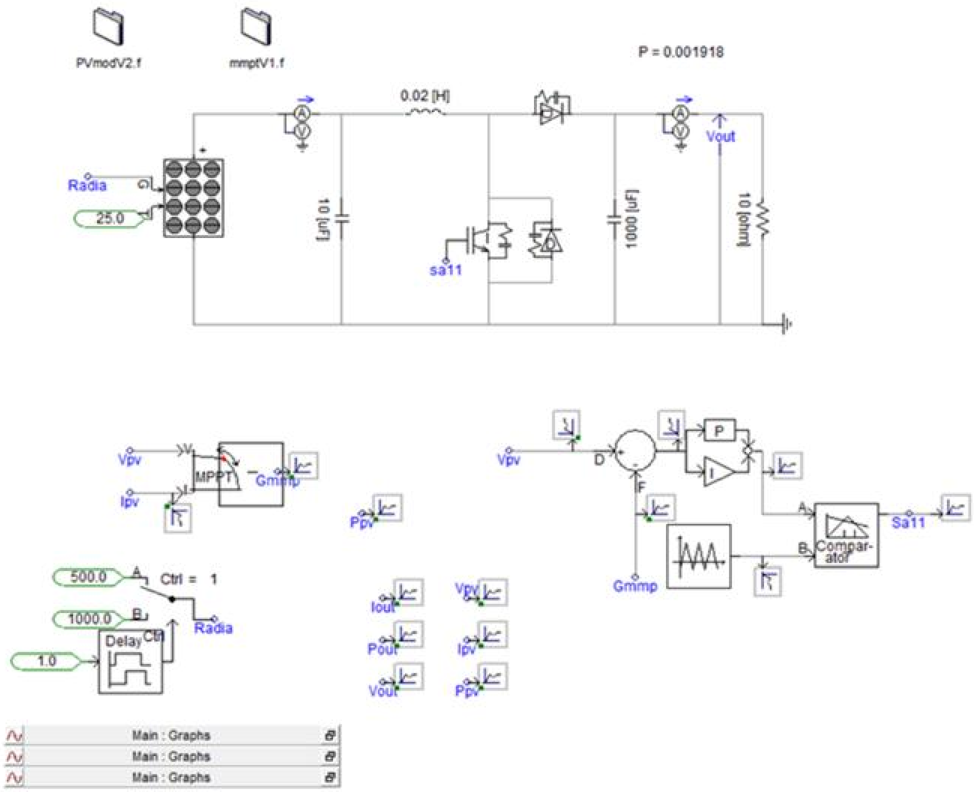

Figure 17. PSCAD simulation diagram of GMPPT with DC-DC converter.

Table 1. Parameters for simulation

PV Module	Value
Maximum Power (P_{MAX})	75 W
Voltage at MPP (V_{MPP})	17.3 V
Current at MPP (I_{MPP})	4.35 A
Open Circuit Voltage (V_{OC})	21.8 V
Short Circuit Current (I_{SC})	4.75 A
Input Capacitor (C_1)	100 [μF]
Inductor(L)	1.2 [mH]
Output Capacitor (C_2)	200 [μF]
Load (R)	60 [Ω]
Switching Frequency (fs)	20 [kHz]

To confirm the power produced during partial shading condition, the load was operated at increased output value and the results are derived. The results related to the power at normal irradiation are as in Figure 18(a), representing solar PV array's module voltage, current, and power. Figure 18(b) shows the results under dynamic irradiation conditions. Under normal irradiation, before reaching the stable operating point, the output of the PV module shows a quick transient response. With only little oscillations, the module and load power settle nearer to their steady state showing effective tracking performance. Under dynamic condition, for sudden changes, the system responds dynamically by maintaining stable operation. With the change from 40 Ω to 80 Ω, the load voltage reduction confirms the adaptability of the converter and control strategy.

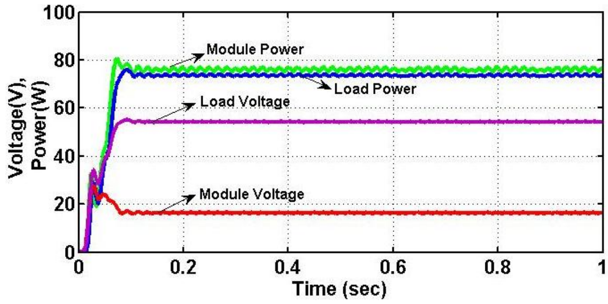

(a) Steady

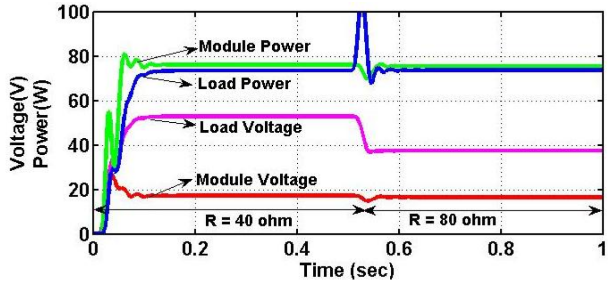

(b) Dynamic States

Figure 18. Voltage and Power Characteristics of Solar PV in Steady and Dynamic States.

Figure 19(a) gives the I-V curves and Figure 19(b) gives the path of GMPPT in x-y plot. With the irradiance of 1000 W/m², there is a non-linear relationship between voltage at the output and current and is shown through I–V characteristics. The validity of the algorithm is confirmed by the successful tracking of the peak point.

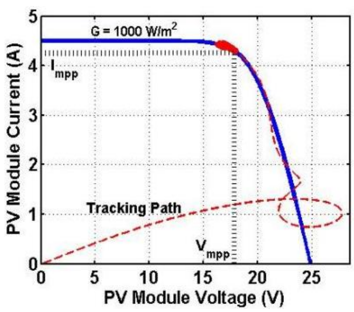

(a) I-V characteristics

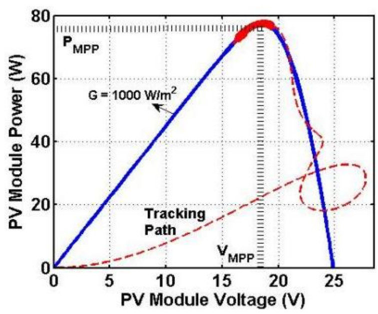

(b) P-V characteristics

Figure 19. Route of MPPT I-V characteristics and P-V characteristics of PV Panel.

To observe the peak power, few samples are taken by the algorithm and during this convergence time, the path of the MPP never get oscillated at any point. The algorithm proved that the convergence occurs at a very less time to attain peak power. Figure 20 shows simulated results.

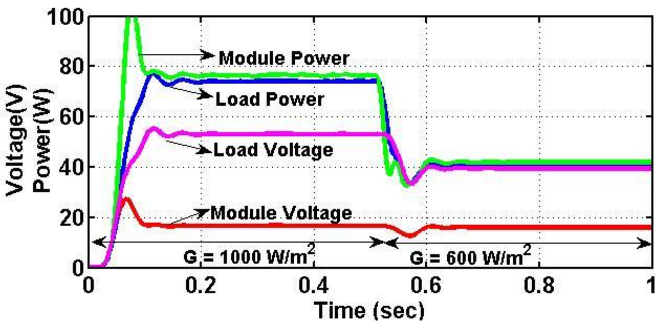

Figure 20. Solar PV under partial shaded condition

From Figure 21, it is evident that even when the module power drops, peak power is restored by the algorithm quickly by identifying the optimal point around 0.55 seconds. Figure 21 gives I-V and P-V curves. Initially, peak current is 2.5A. With irradiation change, power shifts upward, evident in Figure 21(a). Under this condition, MPP shifts to an increased power level. The converter and the MPPT successfully attained a new operating value. Moreover, the effective operation of the control strategy and the consistent operation of the converter is shown through the smooth changeover of the curves. Figure 21(b) clearly highlights peak power. No oscillations occur, confirming faster convergence of the GMPPT algorithm under dynamic conditions. Even with the change in irradiation as well as the sudden change in environmental conditions, the algorithm responds quickly and given a faster convergence. The validity of the proposed MPPT technique to track the peak power is observed through the presented results.

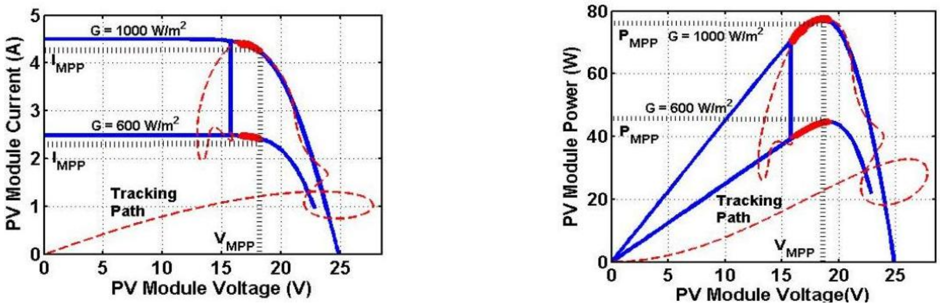

(a) I-V curves (b) P-V curves

Figure 21. Route traced by MPPT with globalized MPPT approach I-V curves and P-V curves

5. Implementation of GMPPT with High Gain Converter for Multiple Solar PV Module

A pictorial representation of the comprehensive circuit setup for MPPT operation using high-gain converter is as in Figure 22. Global MPPT control comprises of 3 distinct control units:

1. Perturb and Observe MPPT control

2.Global MPPT control with stepwise comparison.

Figure 23 shows the PSCAD simulation circuit combining GMPPT and High gain converter.

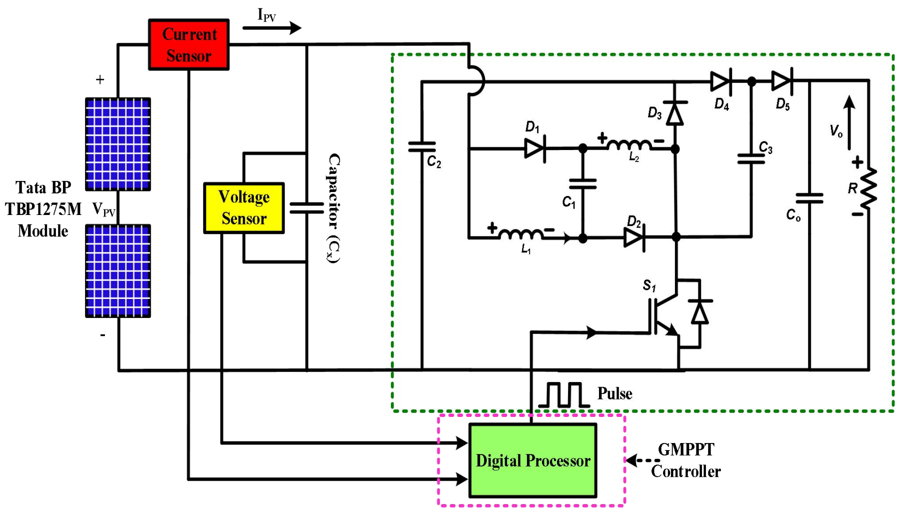

Figure 22. Complete circuit diagram of GMPPT implementation on Hybrid high gain converter.

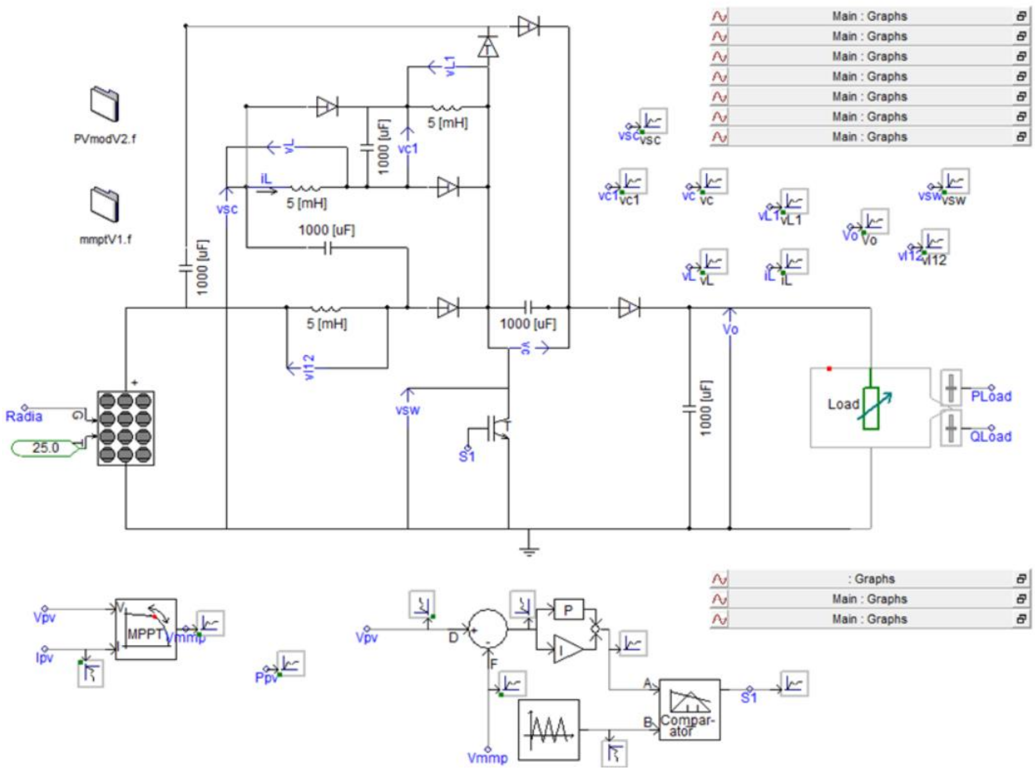

Figure 23. PSCAD Simulation for Implementation of GMPPT in Hybrid High gain Converter.

5.1. P & O MPPT Algorithm:

To find the MPP under normal operating conditions without shading, the algorithm sets the reference voltage (V_{REF}) to 85% of the open-circuit voltage and then it continuously tracks and adjusts the MPP voltage (V_{NMPP}) by employing the P&O method as its primary control strategy.

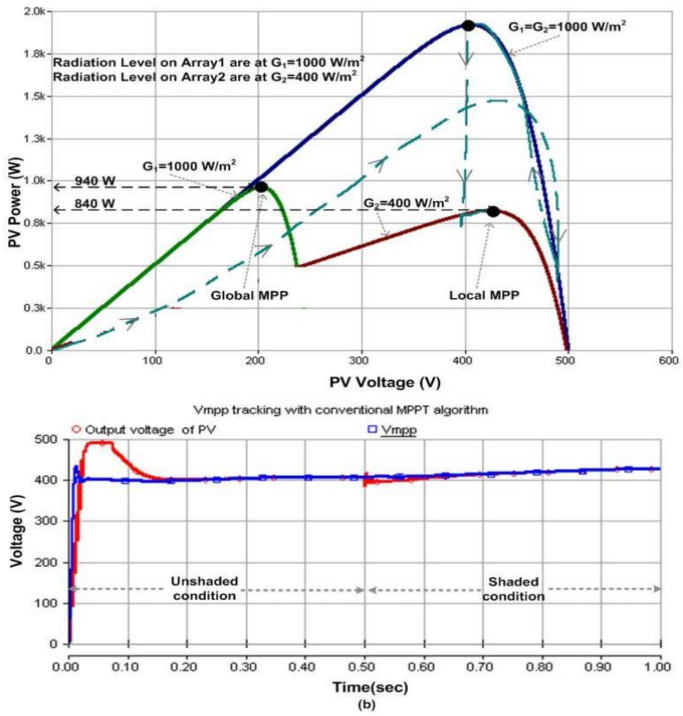

Figure 24. Performance characteristics and VMPP tracking with conventional P&O under variable irradiation.

In this photovoltaic array system, two arrays are used. one receiving irradiance $G_1 = 1000$ W/m² and the second $G_2 = 400$ W/m². When R_L is set to 40 Ω, the duty cycle is optimized to 83% for effective power transfer. As shown in Figure 24, to achieve the peak power point, upon correcting the duty cycle with the sudden load changing conditions, the control algorithm responds quickly. The controller exhibits a fast 20 ms settling time. Under normal operating condition without any shading with P & O method, MPP is reached at $I_{MPP} = 4.57$ A, $V_{MPP} = 420$ V, and $P_{MPP} = 1.92$ kW.

5.2. Global MPPT Control:

In case of intermittent shading, when a timer interrupt arises, the control strategy transitions from the primary algorithm to a comprehensive MPPT framework, thereby implementing a global MPPT control approach. This changeover aims to adapt and follow the new global Voltage (V_{SMPP}) denoted as "t". The algorithm recognizes shading conditions when the change in solar radiation levels among different photovoltaic modules exceeds a predefined threshold. A programmed interrupt is triggered under such circumstances. The GMPPT initiation begins with the setup of the series number of PV modules.

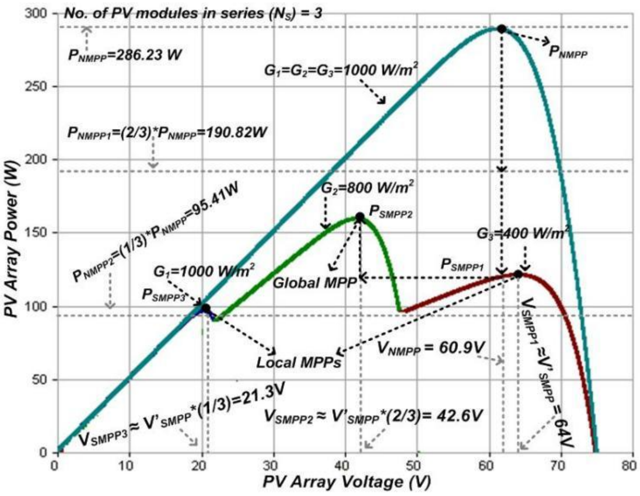

Figure 25. Operating principle of Global MPPT algorithm.

In this condition, one of the photovoltaic module experiences shading conditions. Initially, together PV modules operated at an irradiance level of $G_1 = 1140$ W/m2. Subsequently, shading was manually introduced to the second module, reducing its irradiance to $G_2 = 162$ W/m2. The operational limitations of the traditional P&O algorithm under partial shading conditions are demonstrated in Figure 25. As the standard P&O method cannot navigate shading complexities, it becomes trapped at a local maximum power point (LMPP). Under this condition, the shaded PV module remains unchanged from its unshaded state, resulting in significantly reduced current due to shading and power generation to near zero. The corresponding I-V characteristics for the two series modules under this condition are also illustrated in Figure 25, highlighting the traditional algorithm's inability to trace the global maximum. To overcome this constraint and ensure optimal energy harvesting, the GMPP algorithm is introduced.

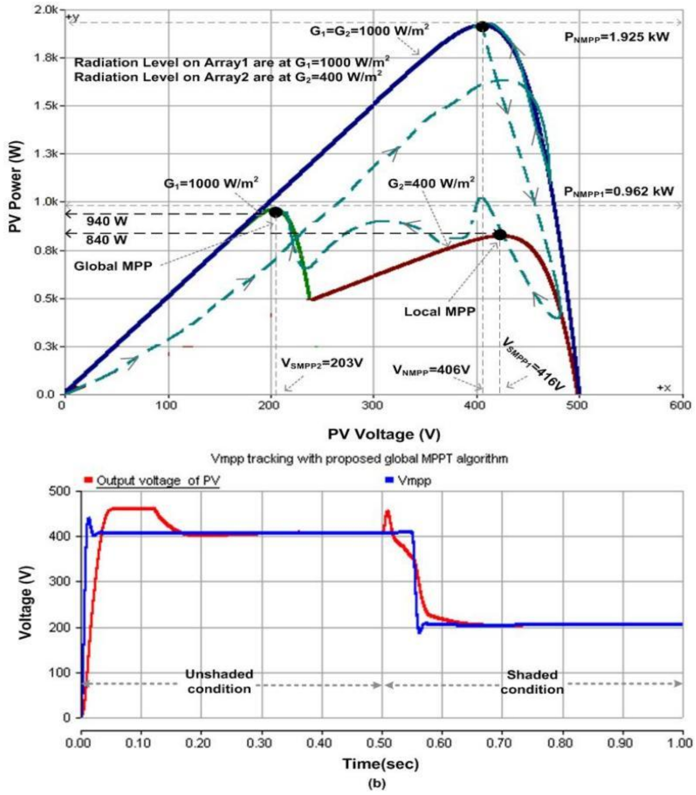

Figure 26. Performance characteristics and VMPP tracking with GMPPT algorithm with changes in irradiation.

Figure 26 validates that when the PV system operates without shading, the conventional P&O algorithm successfully tracks the Peak Power Point. However, when partial shading occurs, the P&O algorithm struggles to follow the Global MPP and remains stuck at the Local MPP. The figure includes a dotted line with an arrow to indicate the path of MPP tracking.

5.3. Performance of Global MPPT with High Gain Converter under different Scenarios:

(a) Unshaded to Partially Shaded Condition:

Initially, when operating under unshaded conditions, all three arrays (G_1, G_2, and G_3) exhibit a uniform value. At this point, the Perturb and Observe algorithm steers the system towards the Maximum Power Point known as P_{NMPP}. However, at t = 0.5 seconds, partial shading occurs, causing the three arrays to experience different radiation levels. Consequently, this introduces three distinct peak points on the Photovoltaic-Voltage curve, as illustrated in Figure 27. Subsequently, it examines if P'_{PV} (t) is less than two-thirds of P_{NMPP} and if this condition is satisfied, leading to a shift to the point. As illustrated in Figure 27, the GMPP is positioned in the right-hand region of the P-V curve.

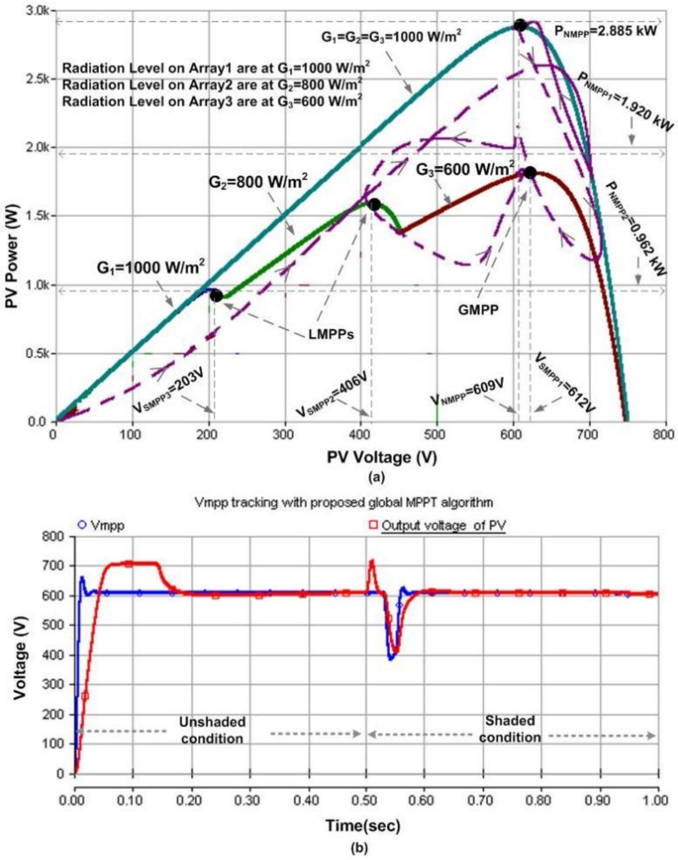

Figure 27. Simulation results of Global MPPT, (a) power voltage characteristics. (b) Tracing of VMPP.

(b) Unshaded to Partially Shaded Condition with Different Irradiation Levels:

Here, the photovoltaic array experiences three different radiation levels. In this scenario, the actual Global Peak Power Point is positioned in the center of the PV curve. Next, it checks if P'_{PV} (t) is less than two-thirds of P_{NMPP}, which is met, and the algorithm shifts to the points. It examines that if the peak power obtained newly is lower than the last peak power, which is not the case in this instance. Therefore, the algorithm remains at the same point, namely, V_{SMPP2}, P_{SMPP2}, which represents the GMPP and is situated at the center of the PV curve, as depicted in Figure 28.

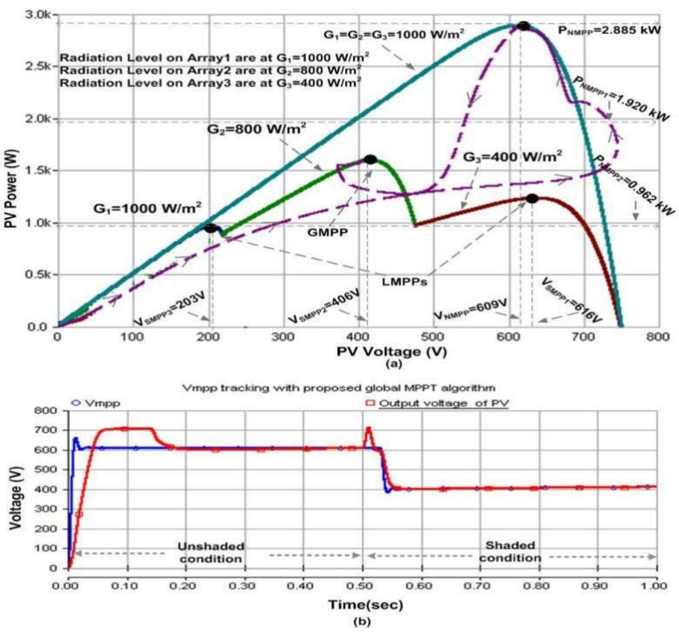

Figure 28. Performance of Global MPPT, (a) Power voltage characteristics. (b) VMPP tracing

(C) Change in Irradiation with all Three Arrays at Equal Irradiation from G_1=1000 W/m2 to G_1=600 W/m2.

All three photovoltaic arrays are exposed to identical radiation levels, with an initial value of G1 = 1000 W/m² during the time interval from t = 0 to 0.5 seconds. Subsequently, in radiation level a sudden change occurs. So that G_1 = 600 W/m² at t = 0.5 seconds. The effectiveness of the GMPPT procedure can be observed in Figure 29.

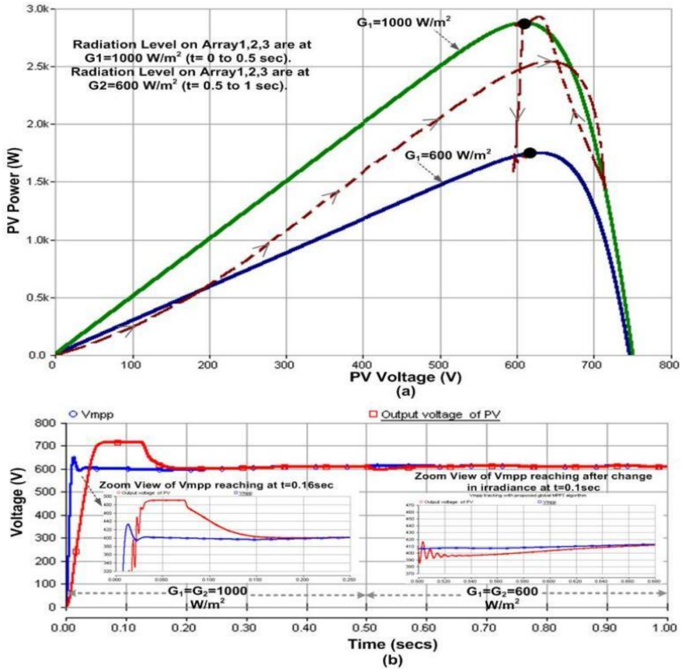

Figure 29. Simulation results of Global MPPT, (a) Power voltage characteristics. (b) VMPP tracing.

Notably, there are no Local MPPs in this scenario, simplifying the task for the controller in locating the Global MPP on the PV characteristic curve. The voltage at the V_{MPP} remains nearly constant under both radiation conditions, but there is a shift in the PV power output level. The controller exhibits precise tracking of the global MPP point and the magnified representation of the V_{MPP} in Figure 29 provides insight into the tracking speed. The transient initial phase has a settling time of approximately 0.16 seconds and it takes about 0.1 seconds to track the V_{MPP} under changing environmental conditions. This demonstrates the algorithm's commendable speed of response.

(D) Partially Shaded to Unshaded Condition with Different Irradiations.

Under this partial shading condition, there exists multiple local MPP's along with a Global MPP. Because of different irradiations, several peaks are formed which makes the tracking more challenging. The proposed GMMPT, successfully tracked the Global peak instead of settling at local peak. The result obtained is clearly depicting the effectiveness of the algorithm.

In this scenario, the photovoltaic array begins its operation with varying levels of shading, specifically G_1 at 1000 W/m2, G_2 at 800 W/m2, and G_3 at 400 W/m2. Initially, the algorithm monitors and follows the GMPP. As depicted in Figure 30, the algorithm tracks the GMPP on the P-V curve and in Figure 30, it shows the tracking of voltage at the operating point V_{SMPP2}, P_{SMPP2}. A sudden variation in irradiance occurs, causing all three PV arrays to return to the same irradiation level, this change triggers an interruption that provides information on all three modules operating under the same radiation level. Consequently, the algorithm promptly adjusts the voltage reference to 85% of V_{OC} allowing it to locate the MPP using the GMPP method with the operating point at V_{NMPP}, P_{NMPP}, as illustrated in Figure 30.

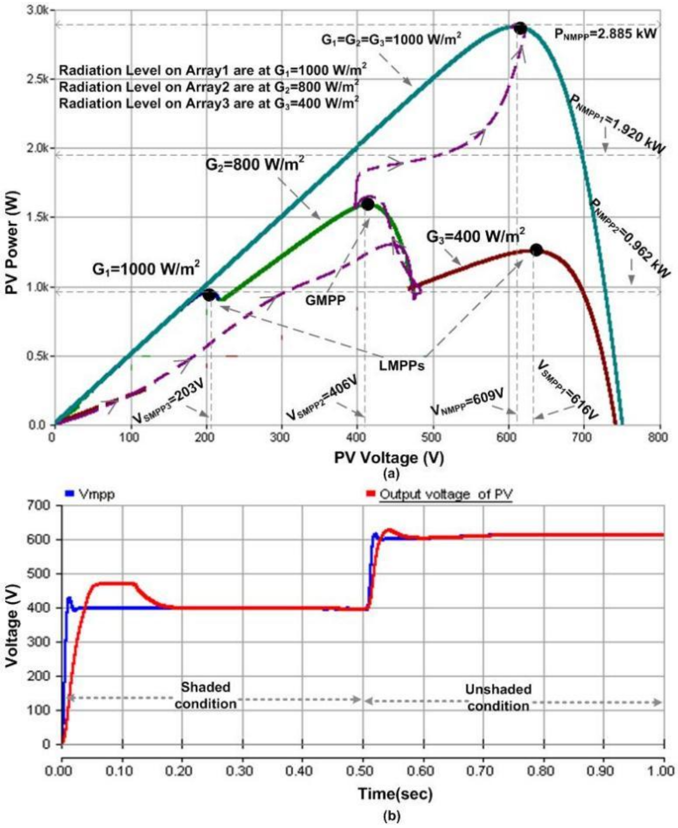

Figure 30. Simulation results of Global MPPT, (a) P-V characteristics. (b) VMPP tracking.

6. Conclusion

The effectiveness of the introduced MPPT algorithm showcased across diverse irradiation conditions, accounting for partial shading effects. This algorithm proficiently monitors and optimizes power by dynamically regulating the duty ratios of the DC-DC converter. The obtained results affirm the commendable performance of the GMPPT algorithm with changing duty cycle, revealing a robust tracing method with enhanced performance in both the steady-state and dynamic conditions. These findings emphasize the algorithm's capability to navigate varying environmental scenarios, making it a hopeful solution for optimizing power extraction in solar photovoltaic systems.

The algorithm is tested under various conditions and the results that are obtained under all the cases proves that the algorithm is effective and giving maximum power under various conditions and the path of the MPP is not deviated at any condition make it a good option to use the algorithm under partial shading conditions effectively.

Conflict of Interest Statement

All authors declare that they have no conflicts of interest.

References

J. Kumar, C. R. Majid, and M. A. Majid, "Renewable energy for sustainable development in India: Current status, future prospects, challenges, employment, and investment opportunities," *Energy, Sustainability and Society*, vol. 10, no. 2, 2020. https://doi.org/10.1186/s13705-019-0232-1.

Y. T. R. Palleswari and R. Vanitha, "A Perspective Study and Remarks of Solar Energy System in India," *Annals of the Romanian Society for Cell Biology*, vol. 25, no. V5, pp. 1335–1347, May 2021.

M. A. Eltawil and Z. Zhao, "MPPT techniques for photovoltaic applications," *Renewable and Sustainable Energy Reviews*, vol. 25, pp. 793–813, 2013. https://doi.org/10.1016/j.rser.2013.05.022.

P. Suresh, G. Kathirvel, T. Kaviyarasu, and P. Aranganadhan, "Critical Sampling Period Determination for an Open-Loop Perturb and Observe MPPT Grid-Connected Solar Photovoltaic System," *International Journal of Engineering Research & Technology (IJERT)*, vol. 12, no. 3, 2023. DOI: 10.17577/IJERTCONV12IS03101.

T. Esram and P. L. Chapman, "Comparison of photovoltaic array maximum power point tracking techniques," *IEEE Transactions on Energy Conversion*, vol. 22, no. 2, pp. 439–449, 2007. https://doi.org/10.1109/TEC.2006.874230.

P. Mohanty, G. Bhuvaneswari, R. Balasubramanian, and N. K. Dhaliwal, "MATLAB-based modeling to study the performance of different MPPT techniques used for solar PV systems under various operating conditions," *Renewable and Sustainable Energy Reviews*, vol. 38, pp. 581–593, 2014. DOI: 10.1016/j.rser.2014.06.001

M. Forouzesh, Y. Shen, K. Yari, Y. P. Siwakoti, and F. Blaabjerg, "High-Efficiency High Step-Up DC–DC Converter with Dual Coupled Inductors for Grid-Connected Photovoltaic Systems," *IEEE Transactions on Power Electronics*, vol. 33, no. 7, 2018. DOI: 10.1109/TPEL.2017.2746750.

J. Ahmed and Z. Salam, "An Enhanced Adaptive P&O MPPT for Fast and Efficient Tracking Under Varying Environmental Conditions," *IEEE Transactions on Sustainable Energy*, vol. 9, no. 3, pp. 1487–1496, 2018. DOI: 10.1109/TSTE.2018.2791968.

S. Mohanty, B. Subudhi, and P. K. Ray, "A New MPPT Design Using Grey Wolf Optimization Technique for Photovoltaic Systems Under Partial Shading Conditions," *IEEE Transactions on Sustainable Energy*, vol. 7, no. 1, pp. 181–188, 2016. DOI: 10.1109/TSTE.2015.2482120

L. Shang, W. Zhu, and P. Li, "Maximum power point tracking of PV systems under partial shading conditions through flower pollination algorithm," *Protection and Control of Modern Power Systems*, vol. 3, article 38, 2018. https://doi.org/10.1186/s41601-018-0111-3.

S. Soedibyo, S. Anam, I. Hafidz, G. R. Zulkarnain, and M. Ashari, "MPPT Design on Solar Farm Using Perturb and Observe Technique Considering Tilt Angle and Partial Shading in Giligenting Island," in *Proc. 2017 International Seminar on Intelligent Technology and Its Applications (ISITIA)*, 2017. DOI: 10.1109/ISITIA.2017.8124084.

S. Titri, C. Larbes, K. Y. Toumi, and K. Benatchba, "A New MPPT Controller Based on the Ant Colony Optimization Algorithm for Photovoltaic Systems Under Partial Shading Conditions," *Applied Soft Computing*, vol. 58, pp. 465–479, 2017. https://doi.org/10.1016/j.asoc.2017.05.017.

S. R. Pendem and S. Mikkili, "Modeling, Simulation and Performance Analysis of Solar PV Array Configurations (Series, Series–Parallel and Honeycomb) to Extract Maximum Power Under Partial Shading Conditions," Energy Reports, vol. 4, pp. 274–287, 2018. https://doi.org/10.1016/J.EGYR.2018.03.003.

R. Rezaii, M. H. Ameri, A. Y. Varjani, and R. Beiranvand, "Overcoming Partial Shading Issue of PV Modules by Using a Resonant Switched Capacitor Converter," in *Proc. 9th Annual Power Electronics, Drives Systems and Technologies Conference (PEDSTC)*, 2018. DOI:10.1109/PEDSTC.2018.8343768.

J. S. K. Goud, R. Kalpana, B. Singh, and S. Kumar, "A Global Maximum Power Point Tracking Technique of Partially Shaded Photovoltaic Systems for Constant Voltage Applications," *IEEE Transactions on Sustainable Energy*, vol. 10, no. 4, 2019. DOI: 10.1109/TSTE.2018.2876756.

G. M. Madhu, C. Vyjayanthi, K. Kolakaluri, and V. Kumar, "A Hybrid PV-Battery Topology to Extract Maximum Power at Partial Shading Conditions for Rural/Remote Area Applications," in *Proc. 2019 International Conference on Computing, Power and Communication Technologies (GUCON)*, 2019.

M. J. Alshareef, "An Effective Falcon Optimization Algorithm-Based MPPT Under Partial Shaded Photovoltaic Systems," *IEEE Access*, vol. 10, pp. 131345–131360, 2022. DOI: 10.1109/ACCESS.2022.3226654.

Bingöl and B. Özkaya, "Analysis and Comparison of Different PV Array Configurations Under Partial Shading Conditions," *Solar Energy*, vol. 160, pp. 336–343, 2018. DOI: 10.1016/j.solener.2017.12.004.

S. Taheri, H. Taheri, Z. Salam, K. Ishaque, and H. Hemmatjou, "Modified Maximum Power Point Tracking (MPPT) of Grid-Connected PV System Under Partial Shading Conditions," in *Proc. 25th IEEE Canadian Conference on Electrical and Computer Engineering (CCECE)*, 2012. DOI: 10.1109/CCECE.2012.6334835

L. T. Alex, V. Jaikrishna, S. S. Dash, and Sridhar, "Design and Analysis of Push-Pull Flyback Interleaved Converters for Photovoltaic Systems," in *Proc. IEEE International Conference on Renewable Energy Research and Applications (ICRERA)*, pp. 757–761, 2017. DOI:10.1109/ICRERA.2017.8191161.

F. M. Shahir, E. Babaei, and M. Farsadi, "Analysis and Design of Voltage-Lift Technique-Based Non-Isolated Boost DC–DC Converter," *IET Power Electronics*, vol. 11, no. 6, pp. 1083–1091, 2018. https://doi.org/10.1049/iet-pel.2017.0259Digital Object Identifier.

A. Smadi, S. Albatran, and M. A. Alsyouf, "A Novel Compact AC/AC Converter for Hybrid Microgrids," in *Proc. IEEE 6th International Conference on Renewable Energy Research and Applications (ICRERA)*, 2017. DOI: 10.1109/ICRERA.2017.8191255.

G. Bharathi, P. Kantharao, and R. Srinivasarao, "Fuzzy Logic Control (FLC)-Based Coordination Control of DC Microgrid with Energy Storage System and Hybrid Distributed Generation," *International Journal of Ambient Energy*, vol. 43, no. 1, pp. 4255–4271, 2022. DOI: 10.1080/01430750.2021.1874526.

M. S. S. Andrade, E. Mattos, L. Schuch, H. L. Hey, and M. L. Silva Martins, "Synthesis and Comparative Analysis of Very High Step-Up DC–DC Converters Adopting Coupled-Inductor and Voltage Multiplier Cells," *IEEE Transactions on Power Electronics*, vol. 33, no. 7, pp. 5880–5897, 2018. DOI:10.1109/TPEL.2017.2742900.

H. Arima, Y. Mizuno, N. Matsui, S. Hattori, and F. Kurokawa, "A Consideration of Model-Based Design of Smart Grid System," in *Proc. 2019 7th International Conference on Smart Grid (icSmartGrid)*, Newcastle, NSW, Australia, pp. 170–173, 2019.DOI: 10.1109/icSmartGrid48354.2019.8990699

B. Krishna and V. Karthikeyan, "Active Switched-Inductor Network Step-Up DC–DC Converter with Wide Range of Voltage Gain at Lower Duty Cycles," *IEEE Journal of Emerging and Selected Topics in Industrial Electronics*, vol. 2, no. 4, pp. 431–441, 2021.DOI: 10.1109/JESTIE.2021.3097943.

K. Bekkam and V. Karthikeyan, "Ultra-Voltage Gain Step-Up DC–DC Converter for Renewable Energy Micro-Source Applications," *IEEE Transactions on Energy Conversion*, 2021. *DOI: 10.1109/TEC.2021.3116076*.

S. Lee and H. Do, "Quadratic Boost DC–DC Converter with High Voltage Gain and Reduced Voltage Stresses," *IEEE Transactions on Power Electronics*, vol. 34, no. 3, pp. 2397–2404, 2019. DOI: 10.1109/TPEL.2018.2842051.

S. Arfin, A. Al Mamun, T. Chowdhury, and G. Sarowar, "Zeta-Based Hybrid DC–DC Converter Using Switched Inductor and Switched Capacitor Combined Structure for High-Gain Applications," in *Proc. of the IEEE International Conference on Power, Electrical and Electronics and Industrial Applications (PEEIACON)*, pp. 1–4, 2019. DOI: 10.1109/PEEIACON48840.2019.9071940.

R. Faraji, E. Adib, and H. Farzanehfard, "Soft-Switched Non-Isolated High Step-Up Multi-Port DC–DC Converter for Hybrid Energy Systems with Minimum Number of Switches," *International Journal of Electrical Power & Energy Systems*, vol. 106, pp. 511–519, 2019. DOI: 10.1016/j.ijepes.2018.10.038.